12-1-2016

CGILS Phase 2 LES Intercomparison of Response of Subtropical Marine Low Cloud Regimes to CO2 Quadrupling and a CMIP3 Composite Forcing Change

Peter N. Blossey
University of Washington, Seattle, pblossey@uw.edu

Christopher S. Bretherton
University of Washington, Seattle

Anning Cheng
Science Systems and Applications, Inc. (SSAI)

Satoshi Endo
Brookhaven National Laboratory

Thijs Heus
Cleveland State University, t.heus@csuohio.edu

AGU PUBLICATIONS

Journal of Advances in Modeling Earth Systems

RESEARCH ARTICLE
10.1002/2016MS000765

CGILS Phase 2 LES intercomparison of response of subtropical marine low cloud regimes to CO_2 quadrupling and a CMIP3 composite forcing change

Peter N. Blossey[1], Christopher S. Bretherton[1], Anning Cheng[2,3], Satoshi Endo[4], Thijs Heus[5], Adrian P. Lock[6], and Johan J. van der Dussen[7]

[1]Department of Atmospheric Sciences, University of Washington, Seattle, Washington, USA, [2]Science Systems and Applications, Inc., Hampton, Virginia, USA, [3]Climate Science Branch, NASA Langley Research Center, Hampton, Virginia, USA, [4]Brookhaven National Laboratory, Upton, New York, USA, [5]Department of Physics, Cleveland State University, Cleveland, Ohio, USA, [6]Met Office, Exeter, United Kingdom, [7]Delft University of Technology, Delft, The Netherlands

Key Points:
- LES intercomparison: more CO_2 lowers, thins marine subtropical low cloud.
- CMIP3 composite climate change forcing also reduces low cloud in all LESs.
- Cloud responses consistent across stratocumulus and shallow cumulus regimes.

Correspondence to:
P. N. Blossey,
pblossey@uw.edu

Citation:
Blossey, P. N., C. S. Bretherton, A. Cheng, S. Endo, T. Heus, A. P. Lock, and J. J. van der Dussen (2016), CGILS Phase 2 LES intercomparison of response of subtropical marine low cloud regimes to CO_2 quadrupling and a CMIP3 composite forcing change, *J. Adv. Model. Earth Syst.*, *8*, 1714–1726, doi:10.1002/2016MS000765.

Received 22 JUL 2016
Accepted 2 OCT 2016
Accepted article online 6 OCT 2016
Published online 27 OCT 2016

Abstract Phase 1 of the CGILS large-eddy simulation (LES) intercomparison is extended to understand if subtropical marine boundary-layer clouds respond to idealized climate perturbations consistently in six LES models. Here the responses to quadrupled carbon dioxide (**"fast adjustment"**) and to a composite climate perturbation representative of CMIP3 multimodel mean $2\times CO_2$ near-equilibrium conditions are analyzed. As in Phase 1, the LES is run to equilibrium using specified steady summertime forcings representative of three locations in the Northeast Pacific Ocean in shallow well-mixed stratocumulus, decoupled stratocumulus, and shallow cumulus cloud regimes. The results are generally consistent with a single-LES study of Bretherton et al. (2013) on which this intercomparison was based. Both quadrupled CO_2 and the composite climate perturbation result in less cloud and a shallower boundary layer for all models in well-mixed stratocumulus and for all but a single LES in decoupled stratocumulus and shallow cumulus, corroborating similar findings from global climate models (GCMs). For both perturbations, the amount of cloud reduction varies across the models, but there is less intermodel scatter than in GCMs. The cloud radiative effect changes are much larger in the stratocumulus-capped regimes than in the shallow cumulus regime, for which precipitation buffering may damp the cloud response. In the decoupled stratocumulus and cumulus regimes, both the CO_2 increase and CMIP3 perturbations reduce boundary-layer decoupling, due to the shallowing of inversion height.

1. Introduction

Going back to the studies of *Cess et al.* [1990], the uncertain response of clouds to climate change has played a leading role in the broad range of global climate model (GCM) estimates of climate sensitivity. In particular, changes in marine boundary-layer clouds in regions of subsidence over the subtropical oceans account for much of the difference in global cloud feedback across models [*Bony and Dufresne*, 2005]. In GCMs, marine boundary-layer clouds are maintained by a tight coupling between radiative cooling, turbulent mixing, and moist physics that is poorly resolved, highly parameterized, and therefore model-dependent. The contrast between these bright, low-lying clouds and the dark ocean beneath allows even small changes in their areal coverage or optical thickness to affect the energy balance of the climate system.

One approach to constraining GCM projections of the future response of clouds to climate change is to establish its relationship to present-day geographical, seasonal, interannual, and interdecadal cloud variations [e.g., *Clement et al.*, 2009; *Dessler*, 2010]. Empirically derived marine boundary-layer cloud-controlling factors in past and present climates should also be relevant for future climate change, but perhaps with different weights. The stratification of the lower troposphere is a good predictor of low cloud fraction in the present-day climate [*Klein and Hartmann*, 1993; *Wood and Bretherton*, 2006]. After accounting for this correlation, interannual variations of low cloud in GCMs and observations are also anticorrelated with SST, both in the subtropical stratocumulus regions [*Qu et al.*, 2014] and when the low cloud regions are defined more broadly [*Myers and Norris*, 2015; *Brient and Schneider*, 2016]. The same dependence of low cloud cover on

stability and SST carries over to GCM climate change simulations, but in that context the SST increases have a stronger influence than the stability changes [*Myers and Norris*, 2016; *Qu et al*., 2015b]. These studies also consider the impacts of other forcing changes, including subsidence, large-scale horizontal advection, surface fluxes, and free-tropospheric humidity. Some aspects of climate change lie outside the current envelope of seasonal and interannual variability, e.g., the impacts of increased CO_2 on the radiative cooling that drives boundary-layer turbulence, although the response of low clouds to overlying cirrus can provide a partial observational proxy [*Christensen et al*., 2013].

Process modeling of low clouds is an important complement to these studies in identifying key cloud-controlling processes for climate change [*Bretherton*, 2015]. If it is sufficiently credible and well-tested, process modeling can provide benchmarks and constraints for parameterization development aimed at ensuring GCMs simulate low cloud feedback processes in a physically correct fashion.

The CFMIP/GASS Intercomparison of Large eddy and Single column models (CGILS) was advanced as a way to understand the physical mechanisms driving low cloud responses to climate in large-eddy simulations (LES) which resolve these low cloud processes and to constrain the responses of these clouds in highly parameterized single column version of GCMs [*Zhang et al*., 2013]. The CGILS framework characterized the equilibrium response of low clouds over the Northeast Pacific to an idealized warming perturbation based on climatological July conditions for three locations with different typical cloud regimes—well-mixed stratocumulus (Sc), decoupled Sc fed by underlying cumulus (Cu), and shallow Cu [*Zhang et al*., 2012]. The warming perturbation, P2S, consisted of a 2 K increase in SST and free-tropospheric temperatures (P2), and a 11% decrease in mean subsidence. While the equilibrium responses of the SCMs to the climate perturbations were affected by their poor vertical resolution and the activity of individual parameterizations [*Zhang et al*., 2013], the LES intercomparison showed more robust agreement among the models, especially for the well-mixed Sc regime, for which the individual responses of the cloud to warming (cloud thinning) and a decrease in subsidence (cloud thickening and a deepening of the MBL) were separately analyzed [*Blossey et al*., 2013]. The net P2S response was a cloud thickening for most LES for the well-mixed Sc case, but varied in sign between models at the decoupled Sc and shallow Cu locations.

To complement this study, *Bretherton et al*. [2013] ran a single LES for an extended set of individual climate perturbations on the CGILS control cases (warming, subsidence, wind speed, free-tropospheric humidity, stability, increased CO_2) as well as a composite climate perturbation, dCMIP3, in which each change was made in proportion to the subtropical mean change in the CMIP3 models with doubled CO_2. For all of the CGILS locations, the composite climate perturbation resulted in cloud thinning, suggesting (unlike the more idealized P2S perturbation) positive low cloud feedbacks on climate change. By evaluating the response to individual climate perturbations, four physical mechanisms underlying the cloud response at the stratocumulus locations were identified, and the consistent cloud decrease compared to P2S could be understood. Stratocumulus cloud thins with warming and with decreased turbulent driving which can result from either weaker radiative cooling (due to increased CO_2 or water vapor aloft) or from weaker surface fluxes (due to weaker winds). Sc thickens in response to weakened subsidence and increased stability. Compared to the CGILS P2S case, the full dCMIP3 response includes the radiative effects of CO_2 and has only half as large a subsidence decrease; both of these favor decreased low cloud in the dCMIP3 case.

These responses have been supported by work in mixed-layer models [*Dal Gesso et al*., 2014; *De Roode et al*., 2014] and in Lagrangian large-eddy simulations of cloud transitions in the Northeast Pacific [*Bretherton and Blossey*, 2014], who also suggested a physical mechanism underlying the cloud thinning response of stratocumulus to warming. The role of precipitation in buffering the response of shallow cumulus to climate perturbations has also been found by *Vogel et al*. [2016]. One limitation of the present framework—the assumption of fixed sea surface temperatures—has been relaxed by *Tan et al*. [2016], who simulated a marine boundary layer atop a slab ocean. Cloud changes in the subtropics can also feedback on the large-scale circulation [*Bony et al*., 2015], unlike in the present framework.

In the present intercomparison study, we identically force a number of LES models with the $4\times CO_2$ and dCMIP3 climate perturbations of *Bretherton et al*. [2013] at the three CGILS locations, and we confirm that their single-LES results are robust. These perturbations were chosen to complement the P2S scenario discussed by *Blossey et al*. [2013], which is analogous to a *Cess et al*. [1990]-type climate perturbation driven by a uniform SST increase. The first perturbation, a quadrupling of CO_2 with fixed SST, is analogous to fast

adjustment of GCMs. The second is a composite climate perturbation combining multiple long-term effects of CO_2 doubling over the eastern subtropical oceans.

2. Model Configuration and Simulations

Six LES groups participated in this intercomparison study. The participating models are described in Appendix B of *Blossey et al*. [2013], and we follow the naming scheme for the models used there. The only model to change substantially since *Blossey et al*. [2013] is DALES, which uses its updated version 4.0 and includes updates to the advection scheme and warm rain microphysics as described in *van der Dussen et al*. [2015]. The S11 simulations using SAMA have been updated from those in *Bretherton et al*. [2013] to correct the subsidence rate, which was stronger than specified by about 5% due to the use of an incorrect density profile in the conversion from vertical pressure velocity ω to vertical velocity w. This affects the equilibrium state of the simulations but has little impact on the response to climate perturbations.

For each of the three CGILS locations, each group submitted a control (CTRL) simulation following the CGILS LES specifications [*Blossey et al*., 2013] and two perturbed simulations. One group, WRF, submitted simulations only for location S6. The first perturbed simulation, $4CO_2$, uses CO_2 quadrupled from the control, with no other forcing changes (and in particular no change in SST), as in *Bretherton et al*. [2013]. The second perturbed simulation, CMIP3 (called dCMIP3 in *Bretherton et al*. [2013]), uses a composite of forcing changes idealized from the subtropical response of CMIP3 models to CO_2 doubling. Following *Qu et al*. [2015a], the CMIP3 forcing was modified to slightly reduce SST in the stratocumulus regions; this has the effect of also increasing stability there. (Stability changes are expressed using estimated inversion strength (EIS) [*Wood and Bretherton*, 2006].) For convenience, Table 1 summarizes the CMIP3 forcing perturbations versus CTRL. The notations $\Delta 4CO_2$ and ΔCMIP3 are used to indicate 8.0–10.0 day mean differences in the model simulations $4CO_2$ minus CTRL and CMIP3 minus CTRL, respectively. Note that UCLA results from S11 are averaged over days 10.0–12.0, rather than days 8.0–10.0, because that model takes longer to approach equilibrium than the other models. This is because UCLA's equilibrium inversion height is comparable to the other models, but for the first few days, it has a smaller entrainment rate w_e and hence a slower rate of boundary-layer deepening $dz_i/dt = w_e + w_{ls}(z_i)$, where z_i is inversion height and w_{ls} is the large-scale vertical velocity.

The specifications of grid spacing, domain size, and so on, also follow *Blossey et al*. [2013]. Except for LaRC, all models used a vertical grid spacing of 5 m with the cloud and inversion layer for the stratocumulus locations S11 and S12, and a horizontal grid spacing of 25 m. For the shallow cumulus location S6, all models used a 40 m vertical and 100 m horizontal grid spacing. The LES models were developed independently and use different advection schemes, except for LaRC, which is derived from an earlier version of UCLA. The CGILS specifications include a bulk surface flux formula used by all models, and a recommendation to use the RRTMG radiative transfer scheme [*Mlawer et al*., 1997] or a functional equivalent.

Figure 1 summarizes the 8.0–10.0 day mean cloud and boundary-layer structure in control simulations of all models at all three locations. Each column shows one LES. The color shading shows the cloud fraction. The black bar to the right of each column marks the inversion height z_i, where the horizontal-mean relative humidity crosses 50%; this height also closely corresponds to the maximum temperature stratification. The gray and orange bars are the lifting condensation level (LCL) of air with the horizontal-mean properties at $0.1z_i$ and $0.9z_i$, respectively. The gray bar falls near the lowest cloud base, and the orange bar lies at the stratocumulus cloud base, if present, or near/above the inversion if there is not a stratocumulus cloud layer.

Table 1. CMIP3 Forcing Perturbations[a]

Location	δSST (K)	$\delta\omega$ (%)	δEIS (K)	δRH_{FT} (%)	δWS (%)
S6	2.5	−5	0.6	−1.5	−1.5
S11	2.25	−5	0.8	−1.5	−1.5
S12	2.2	−5	0.8	−1.5	−1.5

[a]From Table 1 of *Blossey et al*. [2013], except δSST and δEIS are modified at S11 and S12 as discussed in the text.

We define a decoupling index

$$\delta LCL_{10}^{90} = LCL(z = 0.9z_i) - LCL(z = 0.1z_i),$$

which corresponds to the vertical spread between the gray and orange bars; this is an analogue to equation (3) of *Jones et al*. [2011], but using the LCL in the upper part of the boundary layer in place of the

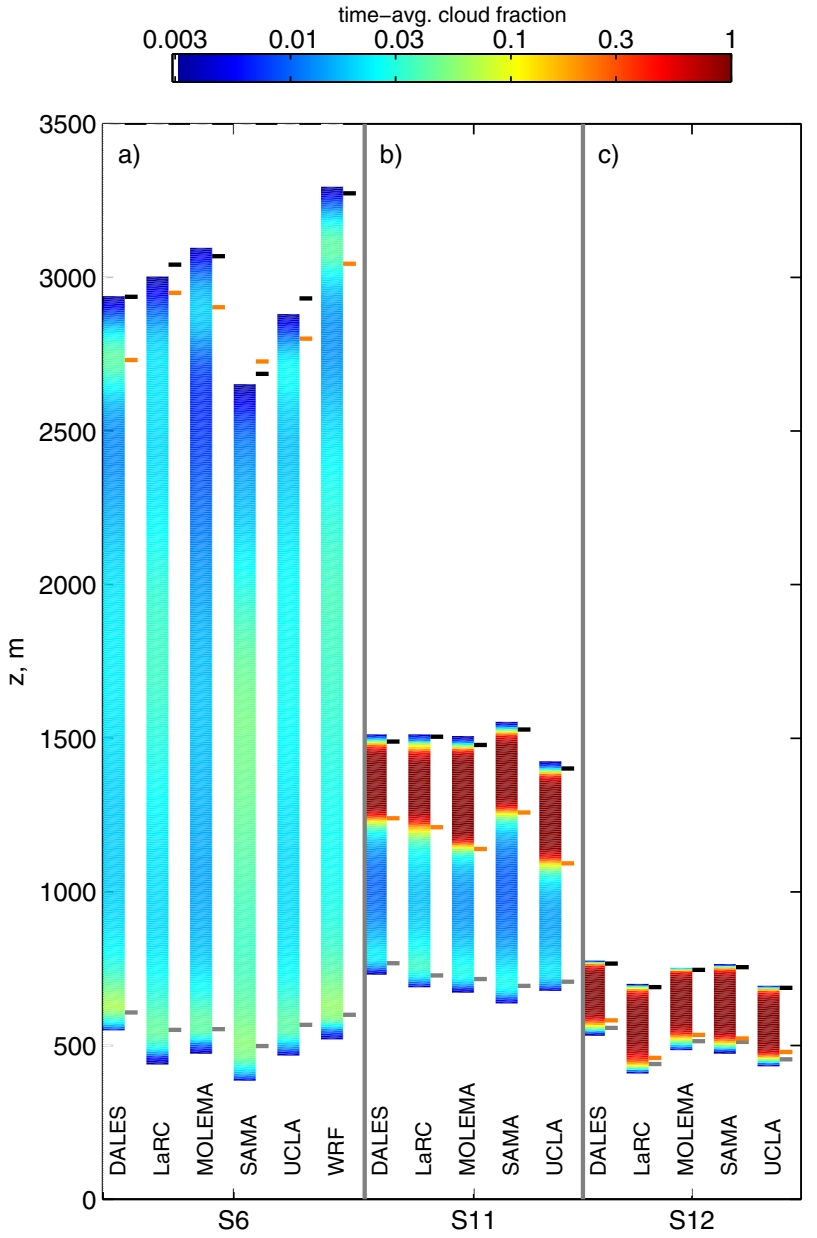

Figure 1. Profiles of cloud fraction from the last 2 days of control simulation with all participating LES models (shaded columns) for (a) S12, (b) S11, and (c) S6. The lines to the right of each shaded column demarcate the corresponding inversion height z_i (black), as well as the LCL computed from boundary-layer properties at $0.1z_i$ (gray) and $0.9z_i$ (orange).

stratocumulus cloud base to allow the measure to be generalized to cases without a stratocumulus cloud layer. If $\delta\mathrm{LCL}_{10}^{90} \approx 0$, as in S12, the cloudy boundary layer is well-mixed. The S11 and S6 locations show increasing degrees of decoupling; the contrast between the cloud regimes in the three locations is clear.

As seen in Figure 1, Table 2, and the results presented in *Blossey et al*. [2013], the control runs of the participating LES have comparable z_i, cloud layer structure, and decoupling statistics at each of the three locations (S6, S11, and S12), and the cloud and boundary-layer states at these locations are easily distinguished from one another. The quantitative differences between the control states at a given location arise from differing choices in numerical discretization and in the parameterization of subgrid turbulence and microphysics through their impact on cloud-top entrainment and precipitation. With similar control states at each location, the cloud response to an identical climate perturbation can be usefully compared because these responses reflect uncertainties with respect to model formulation rather than boundary-layer state (e.g.,

Table 2. CGILS Control, $\Delta 4CO_2$, and ΔCMIP3 Multimodel Statistics[a]

	S6			S11			S12		
Variable	CTRL	$\Delta 4CO_2$	ΔCMIP3	CTRL	$\Delta 4CO_2$	ΔCMIP3	CTRL	$\Delta 4CO_2$	ΔCMIP3
z_i (m)	2990^{+284}_{-304}	-62^{+125}_{-53}	-48^{+67}_{-118}	1481^{+48}_{-79}	$\mathbf{-93}^{+15}_{-8}$	$\mathbf{-73}^{+37}_{-52}$	729^{+38}_{-41}	$\mathbf{-72}^{+26}_{-33}$	$\mathbf{-45}^{+30}_{-31}$
z_b (m)	570^{+271}_{-143}	-48^{+115}_{-217}	-51^{+63}_{-200}	1207^{+69}_{-94}	$\mathbf{-76}^{+28}_{-22}$	-43^{+60}_{-73}	517^{+66}_{-56}	$\mathbf{-50}^{+23}_{-29}$	-20^{+21}_{-28}
LCL_{90} (m)	2859^{+185}_{-133}	-64^{+146}_{-48}	-20^{+75}_{-123}	1188^{+70}_{-95}	$\mathbf{-74}^{+30}_{-24}$	-42^{+65}_{-80}	516^{+66}_{-56}	$\mathbf{-44}^{+26}_{-31}$	-16^{+21}_{-28}
LCL_{10} (m)	563^{+45}_{-65}	-4^{+11}_{-6}	8^{+11}_{-14}	723^{+45}_{-29}	$\mathbf{3}^{+8}_{-3}$	12^{+7}_{-18}	496^{+62}_{-56}	$\mathbf{-49}^{+24}_{-29}$	-20^{+21}_{-28}
Cloud fraction	$0.20^{+0.09}_{-0.07}$	$0.00^{+0.01}_{-0.01}$	$\mathbf{-0.02}^{+0.02}_{-0.02}$	$1.00^{+0.00}_{-0.00}$	$0.00^{+0.00}_{-0.01}$	$0.00^{+0.00}_{-0.00}$	$0.99^{+0.00}_{-0.01}$	$\mathbf{-0.01}^{+0.00}_{-0.01}$	$\mathbf{-0.01}^{+0.00}_{-0.00}$
SHF (W m^{-2})	$8.9^{+3.5}_{-1.7}$	$\mathbf{-0.8}^{+0.4}_{-1.1}$	$\mathbf{-0.7}^{+0.5}_{-0.2}$	$4.6^{+0.6}_{-0.4}$	$\mathbf{-0.7}^{+0.2}_{-0.3}$	$-0.5^{+1.1}_{-0.4}$	$4.9^{+3.0}_{-2.3}$	$0.5^{+0.7}_{-1.1}$	$-0.4^{+0.8}_{-1.1}$
LHF (W m^{-2})	120^{+7}_{-6}	$\mathbf{-2}^{+1}_{-1}$	$\mathbf{14}^{+3}_{-3}$	98^{+6}_{-3}	$\mathbf{-1}^{+0}_{-0}$	$\mathbf{12}^{+1}_{-1}$	82^{+7}_{-6}	$\mathbf{-6}^{+2}_{-3}$	$\mathbf{5}^{+2}_{-3}$
Surf. precip. (mm d^{-1})	$1.0^{+0.1}_{-0.2}$	$-0.1^{+0.2}_{-0.1}$	$\mathbf{0.1}^{+0.1}_{-0.1}$	$0.0^{+0.0}_{-0.0}$	$0.0^{+0.0}_{-0.0}$	$0.0^{+0.0}_{-0.0}$	$0.0^{+0.0}_{-0.0}$	$0.0^{+0.0}_{-0.0}$	$0.0^{+0.0}_{-0.0}$
QOBS (W m^{-2})	97^{+9}_{-10}	$\mathbf{6}^{+2}_{-2}$	$\mathbf{-7}^{+4}_{-4}$	25^{+15}_{-18}	$\mathbf{14}^{+8}_{-13}$	5^{+11}_{-17}	74^{+12}_{-12}	$\mathbf{22}^{+4}_{-3}$	$\mathbf{10}^{+5}_{-6}$
ΔR (W m^{-2})	47^{+5}_{-3}	$\mathbf{-7}^{+2}_{-2}$	-1^{+3}_{-2}	32^{+1}_{-1}	$\mathbf{-4}^{+0}_{-0}$	$\mathbf{-3}^{+1}_{-1}$	42^{+1}_{-1}	$\mathbf{-5}^{+1}_{-2}$	$\mathbf{-5}^{+1}_{-2}$
CTEI parameter κ	$0.49^{+0.11}_{-0.05}$	$0.02^{+0.02}_{-0.03}$	$\mathbf{0.08}^{+0.03}_{-0.03}$	$-0.16^{+0.14}_{-0.09}$	$\mathbf{0.14}^{+0.02}_{-0.04}$	$\mathbf{0.25}^{+0.07}_{-0.07}$	$0.19^{+0.04}_{-0.03}$	$\mathbf{0.06}^{+0.03}_{-0.01}$	$\mathbf{0.14}^{+0.03}_{-0.02}$
w_e (mm s^{-1})	$3.2^{+0.8}_{-0.7}$	$0.0^{+0.6}_{-0.5}$	$-0.1^{+0.3}_{-0.2}$	$4.5^{+0.2}_{-0.3}$	$\mathbf{-0.2}^{+0.0}_{-0.0}$	$\mathbf{-0.3}^{+0.1}_{-0.1}$	$3.9^{+0.2}_{-0.2}$	$\mathbf{-0.5}^{+0.1}_{-0.1}$	$\mathbf{-0.5}^{+0.1}_{-0.1}$
w_*^3 (m^3 s^{-3})	$0.97^{+0.20}_{-0.22}$	$-0.05^{+0.08}_{-0.05}$	$0.02^{+0.06}_{-0.07}$	$0.66^{+0.17}_{-0.09}$	$\mathbf{-0.09}^{+0.02}_{-0.02}$	$-0.02^{+0.13}_{-0.06}$	$0.55^{+0.07}_{-0.04}$	$\mathbf{-0.08}^{+0.01}_{-0.03}$	$\mathbf{-0.08}^{+0.01}_{-0.01}$
Δb (m s^{-2})	$0.16^{+0.02}_{-0.05}$	$0.00^{+0.01}_{-0.01}$	$0.00^{+0.01}_{-0.01}$	$0.31^{+0.01}_{-0.03}$	$\mathbf{-0.01}^{+0.01}_{-0.01}$	$-0.01^{+0.01}_{-0.01}$	$0.34^{+0.01}_{-0.01}$	$\mathbf{-0.01}^{+0.00}_{-0.01}$	$\mathbf{-0.01}^{+0.00}_{-0.01}$
LWP (g m^{-2})	26^{+7}_{-7}	-1^{+1}_{-1}	0^{+0}_{-0}	63^{+24}_{-15}	-8^{+12}_{-8}	-13^{+14}_{-14}	42^{+7}_{-11}	$\mathbf{-9}^{+2}_{-3}$	$\mathbf{-9}^{+3}_{-2}$
SWCRE (W m^{-2})	-24^{+6}_{-7}	1^{+2}_{-1}	$\mathbf{2}^{+1}_{-1}$	-167^{+20}_{-25}	$\mathbf{12}^{+8}_{-12}$	$\mathbf{18}^{+10}_{-15}$	-142^{+21}_{-15}	$\mathbf{16}^{+4}_{-3}$	$\mathbf{19}^{+5}_{-7}$
LWCRE (W m^{-2})	2^{+1}_{-0}	0^{+0}_{-0}	0^{+1}_{-1}	15^{+3}_{-2}	-2^{+2}_{-1}	$\mathbf{-2}^{+1}_{-1}$	7^{+4}_{-2}	$\mathbf{-1}^{+0}_{-1}$	$\mathbf{-1}^{+0}_{-1}$

[a]Each entry is the multimodel mean, with the superscript indicating the most positive deviation of an individual LES from that mean, and the subscript the most negative deviation. Variables are defined in the text.

well-mixed versus decoupled). As subtropical cloud feedbacks in GCMs are so diverse, we judge the LES responses to be a useful constraint for GCMs if they agree in their sign and not in magnitude. While this standard for agreement is relatively weak (the interquartile range of the SWCRE response to a given perturbation would be a more robust quantitative metric), we feel that it is justified by the large uncertainty in GCMs realizations of these cloud responses. One weakness of the present set of CGILS cases is that the two stratocumulus locations (S11 and S12) have full cloud cover in all simulations, so that stratocumulus cloud fraction changes (which make up an important part of stratocumulus cloud feedbacks in GCMs) are not accessible in the current CGILS framework.

3. Results: $4CO_2$ and CMIP3 Perturbations

Results for the control case and both forcing perturbations for the three locations are summarized in Table 2. Each tabulated value is a multimodel mean; for a perturbation, it is shown in **bold** if all LES agree on the sign of the change. The superscript and subscript indicate the most positive and negative deviations of an individual LES from that mean, as an indication of intermodel spread. One expected result documented by the table is that longwave cloud radiative effect (LWCRE) and its perturbation-induced changes are much smaller in all models than SWCRE, so that SWCRE changes are a good proxy for changes of net top-of-atmosphere radiative effect in these boundary-layer cloud regimes.

3.1. Well-Mixed Stratocumulus (S12)

Figure 2a shows the simulated changes in SWCRE and z_i at S12 due to the two perturbations, following the format of *Blossey et al.* [2013]. In this well-mixed stratocumulus regime, the LES all respond very similarly. They exhibit a lowering of the inversion and considerably less negative SWCRE, though the magnitude of the responses differ considerably between the models. The inversion lowering is stronger, 50–100 m, for $4CO_2$, while the SWCRE change ranges from 13 to 20 W m^{-2} for both perturbations. For one representative LES (MOLEMA), 6 hourly means from days 2.0 to 10.0 of the evolution to the steady state are also plotted for the three cases as thick light curves. The gray curve in particular shows the SWCRE becoming slightly more negative as the inversion slowly deepens. This "slow manifold" dependence of SWCRE on inversion height alone clearly contributes to the difference between SWCRE in the control and perturbed simulations, but certainly does not explain all of the SWCRE response to the CMIP3 perturbation. As described in *Bretherton et al.* [2010], the cloud-top boundary layer approximately follows a slow manifold after the relatively fast (∼1 day) adjustment of its internal dynamics (e.g., cloud base height) to the present boundary-layer depth and entrainment rate, but before its entrainment rate comes into equilibrium with

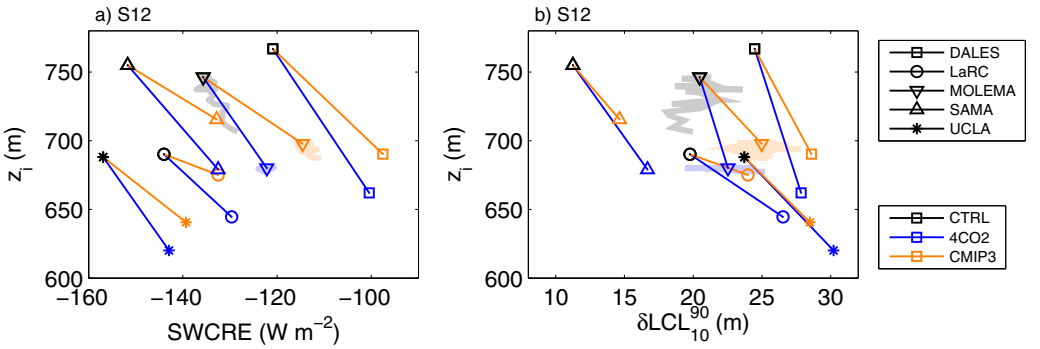

Figure 2. $\Delta 4CO_2$ and ΔCMIP3 responses for the well-mixed stratocumulus regime (S12): (a) inversion height and SWCRE and (b) inversion height and δLCL_{10}^{90}. Light shaded lines show the "slow-manifold" response of MOLEMA, plotted every 6 h from days 2.0 to 10.0.

the large-scale subsidence (over ∼5–10 days). The slow-manifold response is similar for other LES, so we only show it for one model.

Bretherton et al. [2013] analyzed the physical mechanisms responsible for these responses, based on results from the SAM LES alone. They attributed the $\Delta 4CO_2$ response to the weaker cloud-top radiative cooling of the PBL due to increased downwelling longwave radiation. This leads to less turbulence and entrainment, and hence a lowering of both the inversion and cloud base. The turbulence is generated by the vertical integral of the buoyancy flux, which must, therefore, also reduce in proportional to the radiative cooling. In both an LES and a mixed-layer model, this reduction is accomplished through roughly proportional shrinkage of the cloud and subcloud layer depths, with little change in the buoyancy fluxes within either region. That is, the stratocumulus cloud layer thins in response to enhanced CO_2. Note that this "proportional thinning" argument does not work for other forcing perturbations such as subsidence or wind-speed changes, for which the buoyancy fluxes do change in the two layers in ways unique to each perturbation. Hence, the cloud thickness response to each perturbation has to be separately analyzed in a full mixed-layer model or LES.

Table 2 shows that indeed, in each LES the boundary-layer radiative flux divergence ΔR is reduced by about 5 W m^{-2} (12%) due to the quadrupling of CO_2, and that the liquid water path (LWP), the boundary-layer integrated buoyancy production of TKE (expressed as w_*^3) and the entrainment rate w_e are similarly reduced, with rather little intermodel scatter. Thus, the LES as a group robustly demonstrates the direct radiative effect of a CO_2 increase on lowering and thinning a well-mixed stratocumulus layer by reduced driving of convection. The radiative cooling ΔR is affected by the boundary-layer cloud distribution, depth, and thermodynamic profiles, so it is not a purely external parameter and can be expected to vary somewhat between simulations of the same case with different LES models. However, those prove to be minor issues in the S12 case.

The changes in inversion temperature and humidity jumps induced by the $4CO_2$ perturbation are modest. There is a slight decrease of temperature just above the inversion, which causes a slight but systematic decrease in the inversion buoyancy jump Δb in the models and a slight increase in the moist instability parameter $\kappa = 1 + c_p \Delta\theta_l / L\Delta q_t$ (Table 2). This supports the interpretation that the entrainment rate reductions mainly reflect reduced turbulence rather than changed inversion stability.

The CMIP3 perturbation involves a much more complex mixture of forcing changes, but ΔR is reduced by a comparable amount to $4CO_2$ (Table 2), now due to the combined greenhouse effects of CO_2 doubling and more water vapor aloft. The change in SWCRE is also comparable, but *Bretherton et al*. [2013] suggest that this change is not just radiatively driven. Their Figure 5 suggests two other important but counteracting contributors are reduced subsidence and the thermodynamic effect of column warming, which thicken and thin the cloud layer, respectively.

Table 2 shows that for CMIP3, buoyancy production, and entrainment are reduced comparably to the $4CO_2$. Although the CTEI parameter κ increases by around 0.14 for all models due to the larger inversion humidity jump associated with a warmer atmospheric column, this does not appear to increase entrainment efficiency in CMIP3 compared to $4CO_2$, corroborating *Bretherton et al*. [2013] and *Bretherton and Blossey* [2014].

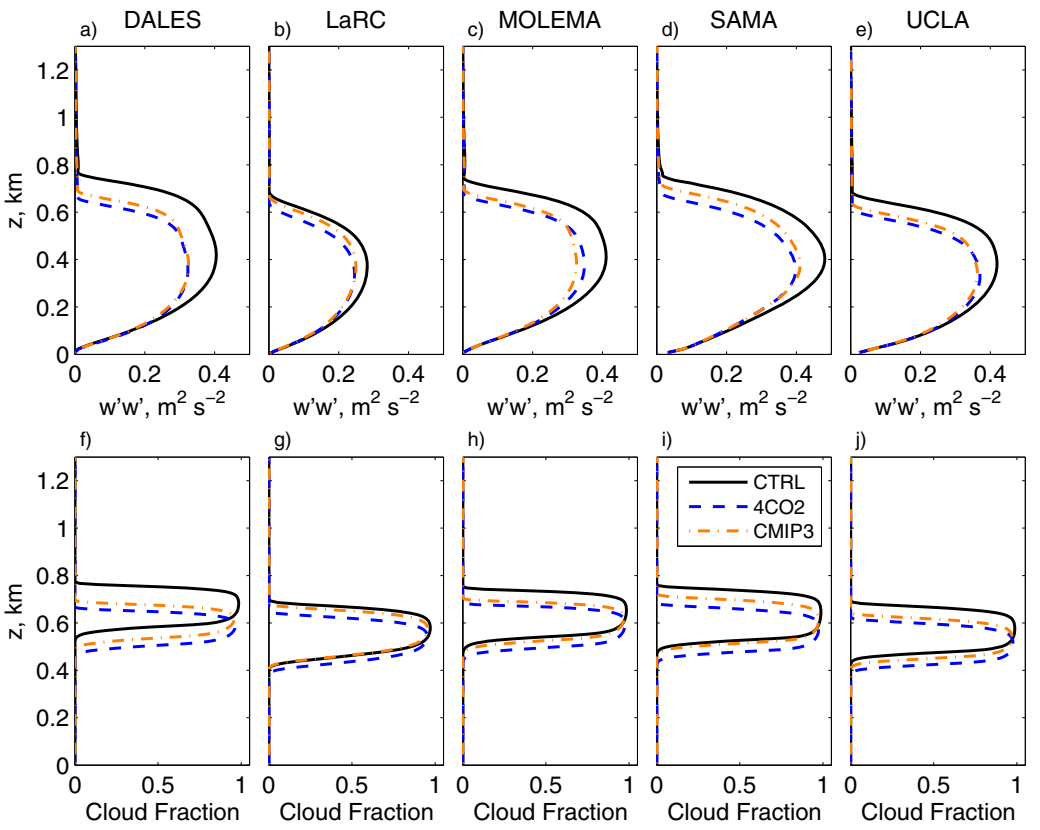

Figure 3. S12 control, $4CO_2$, and CMIP3 8.0–10.0 day mean profiles of (a–e) vertical velocity variance and (f–j) cloud fraction for the LES models.

Figure 2b shows the perturbations in the decoupling parameter. In all models, δLCL_{10}^{90} increases very slightly (by 2–7 m) but remains very small (<30 m) for both perturbed cases, consistent with a well-mixed layer. The slow-manifold evolution for the MOLEMA simulations suggests that these tiny δLCL_{10}^{90} increases reflect the perturbed thermodynamic driving of the boundary layer rather than changes in boundary-layer structure associated with inversion height differences between the simulations.

Figure 3 shows the vertical velocity variance and cloud fraction profiles simulated for S12 by the models in the control, $4CO_2$, and CMIP3 scenarios. All models exhibit a single maximum of $\overline{w'w'}$ near cloud base for all scenarios, characteristic of a well-mixed layer, but the maximum is clearly weaker for both perturbed scenarios than for the control run.

3.2. Decoupled Stratocumulus (S11)

In the decoupled stratocumulus regime of S11, the LES SWCRE and z_i responses to the two perturbations are qualitatively similar to S12, but more scattered (Figure 4a). As for S12, the perturbations both reduce boundary-layer radiative cooling by 3–4 W m^{-2} (10%) in all models due to increased downwelling longwave radiation. This drives reduced buoyant TKE production (w_*^3) and a 5% entrainment reduction (Table 2). As a result, all LESs simulate a lowering of the inversion in response to both perturbations, ranging from 85 to 110 m for $4CO_2$ and 35 to 125 m for CMIP3 (where there is partial compensation by reduced subsidence). Their SWCRE generally becomes less negative, with a range of 0–20 W m^{-2} for $4CO_2$ and 3–28 W m^{-2} for CMIP3. The $\Delta 4CO_2$ and ΔCMIP3 SWCRE changes for our representative LES, MOLEMA, are not aligned with its control slow-manifold behavior, which show very little sensitivity of SWCRE to inversion height changes alone.

It has been suggested that subtropical marine boundary layer will become more decoupled in a warmer climate due to the larger humidity difference between the ocean surface and the free troposphere and increasing latent heat fluxes [e.g., *Brient and Bony*, 2012]. Our results suggest the opposite for S11 (as well as

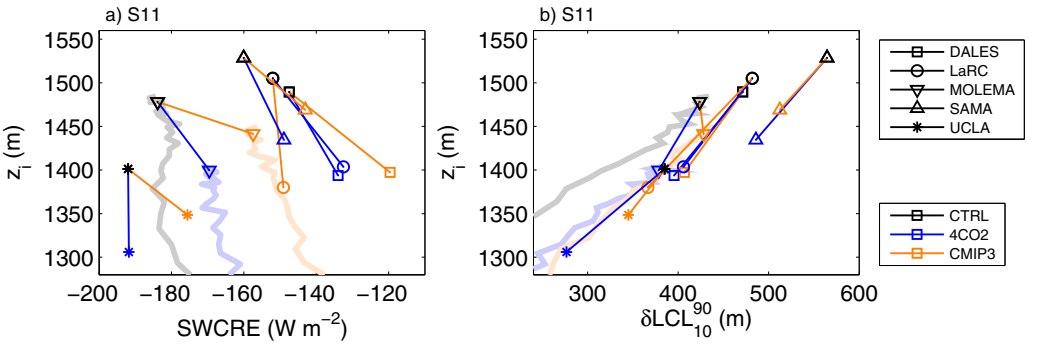

Figure 4. As in Figure 2, but for the decoupled stratocumulus regime (S11).

S6). Instead, we find that changes in δLCL_{10}^{90} respond primarily to changes in boundary-layer depth. Figure 4b shows that δLCL_{10}^{90} decreases for both climate perturbations in all the LES, and that this decrease is highly correlated with the inversion height decrease. The thick, gray slow-manifold curve for MOLEMA shows that this behavior is explained by the change in cloud-topped boundary-layer structure associated with a shallower inversion, without any forcing changes.

Figure 5 shows the S11 vertical velocity variance and cloud fraction profiles for the control and perturbed simulations. As for S12, consistent with the reduced buoyant driving of turbulence, there is a reduction in the maximum vertical velocity variance in the cloud layer for both perturbations, except for the UCLA model with the $4CO_2$ perturbation (for which the Sc do not thin, unlike the other LES). In the surface-driven mixed layer below the cumulus cloud base, there is very little change in vertical velocity variance for either perturbation.

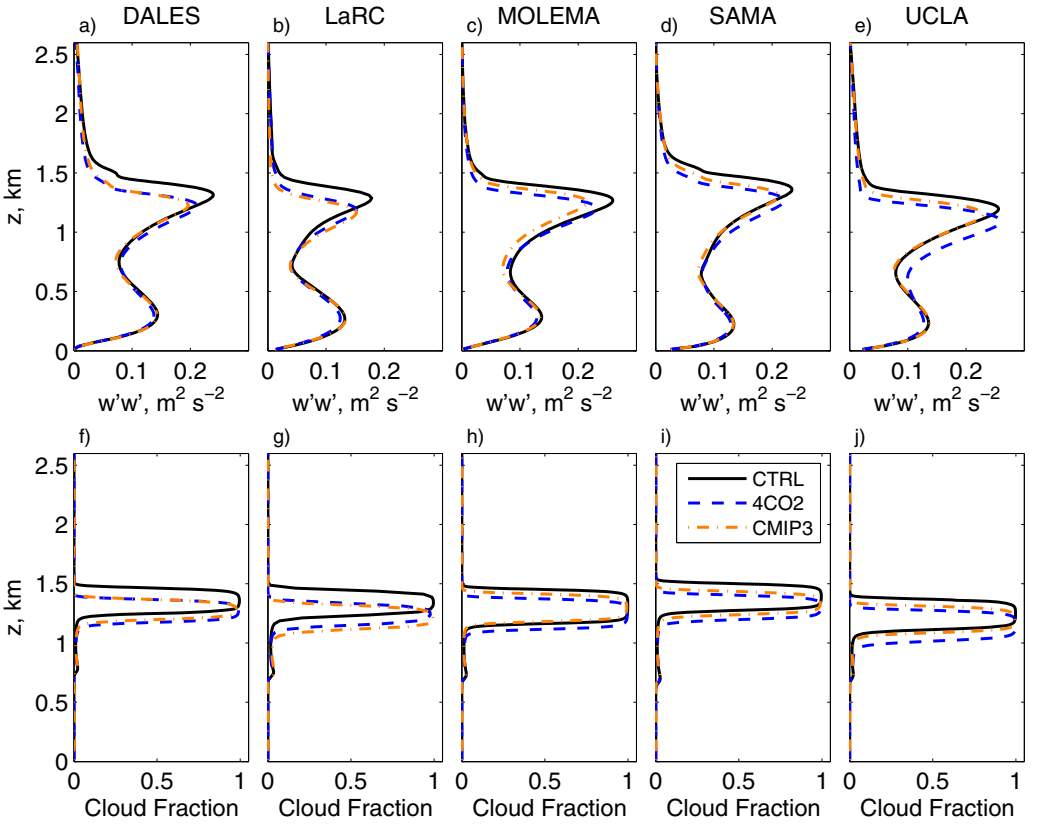

Figure 5. As in Figure 3, but for the decoupled stratocumulus regime (S11).

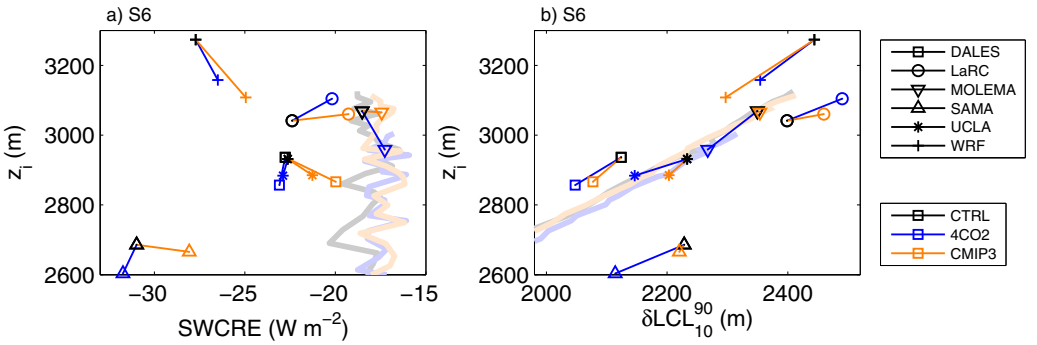

Figure 6. As in Figure 2, but for the precipitating shallow cumulus regime (S6).

Entrainment rate is reduced more by CMIP3 than in $4CO_2$ even though (as with S12) the moist instability parameter κ increases much more than for $4CO_2$ (Table 2) and other factors like w_*^3 and the inversion buoyancy jump also do not explain the entrainment reduction. Again, this argues against κ increases driving cloud thinning in a warming climate via more efficient entrainment.

3.3. Shallow Cumulus (S6)

At S6, the cloud fraction is much smaller and the radiative destabilization of the boundary layer is substantially driven by clear-sky processes. Hence, the $4CO_2$ perturbation considerably reduces the radiative cooling for all models, but unlike at S11 and S12 the CMIP3 perturbation does not (Table 2). Instead, the increased specific humidity of the boundary layer and the increased emissivity of the free troposphere have largely opposing effects on ΔR.

Another difference from the other locations is the presence of significant precipitation at S6 (Table 2). *Bretherton et al*. [2013] and *Seifert et al*. [2015] suggested that in a precipitating shallow cumulus regime such as simulated in S6, a precipitation governor mechanism helps regulate the cloud layer depth and inhibits large changes in the boundary-layer depth, structure, and cloud cover in response to forcing perturbations. Indeed, the $\Delta 4CO_2$ and ΔCMIP3 changes in inversion height are modest in proportion to the boundary-layer depth and are accompanied by small precipitation changes (Table 2 and Figure 6a). For $4CO_2$, five of the six LES have decreases in both precipitation (from -0.1 to -0.2 mm d^{-1}) and inversion height (-50 to -120 m), while both inversion height and precipitation increase in the remaining model, LaRC, by 60 m and 0.1 mm d^{-1}, respectively. For CMIP3, the inversion height changes range from -160 to 20 m but are accompanied by a slight increase in precipitation.

The changes in SWCRE in all models are weak for both perturbations (Figure 6a). For $4CO_2$, the SWCRE change is 0–2 W m^{-2}. For CMIP3, all LES suggest a slightly less negative SWCRE. Perturbations to LWP, cloud fraction, buoyancy production, and entrainment rate are also small in all models (Table 2). Figure 6b shows that even more clearly than for S11, the decoupling metric changes in lockstep with the inversion height for both perturbations, following the lightly shaded slow-manifold curves.

Figure 7 shows that the S6 vertical velocity variance and cloud fraction profiles are remarkably similar for the control versus perturbed simulations of most LESs, except right at the top of their cloud layers where ΔCMIP3 decreases in cloud fraction correspond to the modestly positive changes in SWCRE for CMIP3. A similar result for the P2S perturbation considered in the CGILS Phase 1 intercomparison was shown in Figure 22 and Table 5 of *Blossey et al*. [2013].

3.4. Surface Energy Balance

Table 2 shows that for all three locations, there is a slight decrease in latent heat flux (LHF) for $4CO_2$ and a larger 5–15% increase for CMIP3 in all models. The change in sensible heat flux (SHF) is small, less than 1 W m^{-2} in the multimodel mean for all locations and both perturbations. This results in a slight increase in surface buoyancy flux for CMIP3.

The perturbation to the net energy flux into the ocean, labeled QOBS in Table 2, suggests how a mixed-layer ocean would respond to the changes in the overlying atmosphere and cloud-topped boundary layer. For the $4CO_2$ perturbation, in which SST is artificially fixed, we might expect an increase in QOBS which

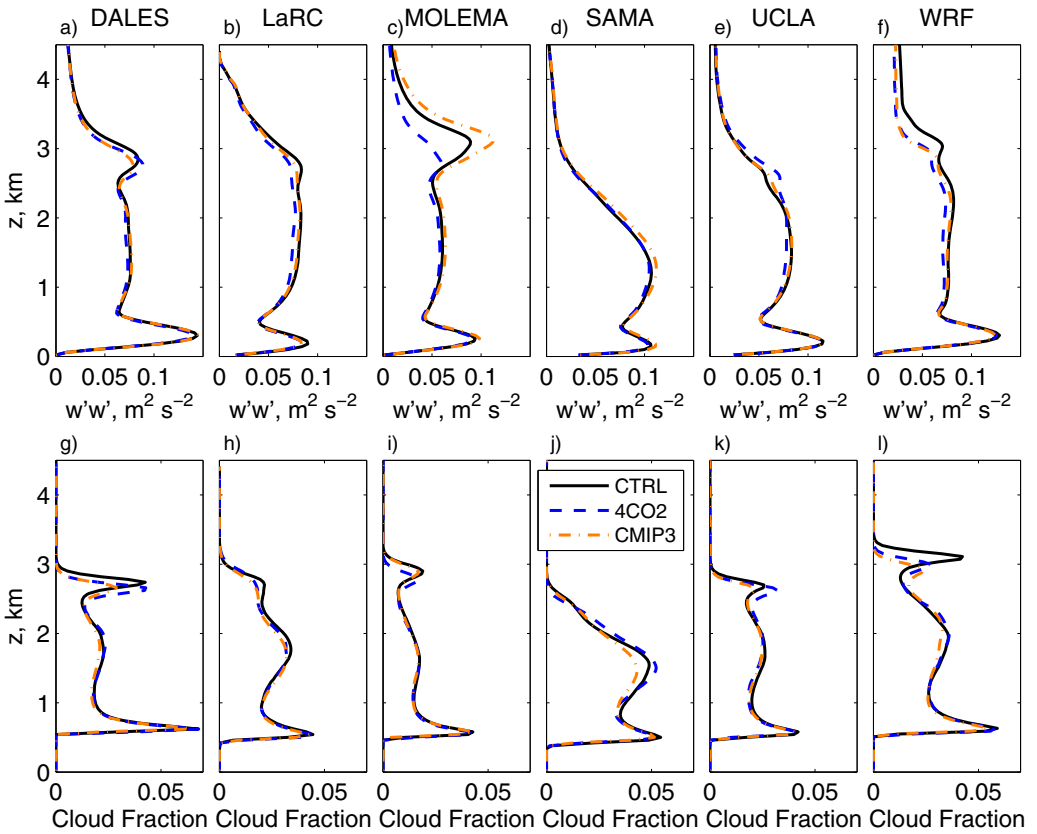

Figure 7. S6 control, $4CO_2$, and CMIP3 8.0–10.0 day mean profiles of (a–f) vertical velocity variance and (g–l) cloud fraction for the LES models.

would start warming the ocean surface. All LES models at all locations do indeed simulate such an increase, ranging from 4 to 8 W m^{-2} at S6, from 1 to 22 W m^{-2} at S11, and 19 to 26 W m^{-2} at S12. The change in downwelling shortwave flux dominates the intermodel spread in QOBS.

For the CMIP3 perturbation, one might hope that all the forcing changes are consistent with the specified SST change, such that the QOBS change is approximately zero. At S11, the QOBS changes from the models do indeed scatter around zero. For S12, they are positive (4–15 W m^{-2}) in all the models, while for S6 they are negative (-3 to -11 W m^{-2}) for all the models. To maintain the specified SST change at S6 or S12 would thus require slightly different perturbations to wind speed, horizontal heat and moisture advection, or ocean heat flux divergence than the present case specifications. The frameworks advocated by *Caldwell and Bretherton* [2009] for a mixed-layer model and *Tan et al.* [2016] for large-eddy simulation allow the exploration of low cloud responses under conditions of fixed ocean heat flux divergence rather than with prescribed SSTs.

4. Conclusions

This second phase of the CGILS LES intercomparison shows that boundary-layer clouds simulated by six independent LES models respond consistently to two climate perturbations relevant to greenhouse warming across three subtropical climate regimes, well-mixed Sc, Cu under Sc, and precipitating shallow Cu. It corroborates the single-LES results of *Bretherton et al.* [2013] for similar perturbations, as well the physical interpretations for these responses offered therein.

The first perturbation, $4CO_2$, idealizes the fast adjustment of the boundary layer to a CO_2 quadrupling before SST can respond. This induces a shallowing of the inversion in all the models for the two Sc regimes. With the exception of a single model at S11, the cloud also thins, inducing a 0–10% SWCRE reduction depending on the model. We interpret this as a response to increased downwelling longwave radiation

from the additional CO_2 in the free troposphere. For the shallow Cu regime, the inversion height also drops slightly in most models, but the cloud changes are small.

The second perturbation, CMIP3, is a composite forcing change combining perturbations in SST, subsidence, inversion stability, surface winds, and free-tropospheric humidity under CO_2 doubling suggested by the CMIP3 models. In the Sc regimes, it induces an inversion lowering and cloud thinning generally similar to CO_2 quadrupling. In all regimes, including shallow Cu, this perturbation induces a 0–15% reduction in SWCRE magnitude (implying positive cloud feedback) for all LES models. As with the $4CO_2$ perturbation, the size of the predicted SWCRE change varies considerably across models even though its sign is consistent.

The CMIP3 perturbation corresponds roughly to half of the long-term climate change expected from CO_2 quadrupling. Since the cloud reductions from CMIP3 are slightly larger than those from $4CO_2$ for most LES and in most regimes, this suggests that the fast adjustment might contribute somewhat under half of the overall cloud response to greenhouse warming in these subtropical boundary-layer cloud regimes. The LES simulations of *Bretherton and Blossey* [2014] find that the cloud reductions due to quadrupled CO_2 account for much less than half those found when increases in CO_2 and warming (with SSTs increased by 4 K) are combined. However, the latter simulation displayed nonlinearities in the cloud response with less than full cloud cover, while the more modest changes associated with the CMIP3 perturbation here seem to be, roughly, a linear superposition of the individual perturbations, as seen for SAMA in *Bretherton et al*. [2013].

In a warmer climate with a similar inversion strength but a larger humidity difference between the sea surface and the free troposphere, one might anticipate more decoupling and/or evaporative enhancement of entrainment, which might lead to drying of the upper part of the boundary layer and explain why there is less stratocumulus cloud. Our results for the CMIP3 scenario do not support these explanations of the cloudiness decrease. On contrary, we find that outside of the well-mixed Sc regime, our measure of decoupling is primarily tied to inversion height. Hence, inversion height decreases in almost all models lead to decreased decoupling. Furthermore, although the instability parameter κ increases in the warmer climate, entrainment rate decreases in all models at all locations. The CMIP3 w_e reduction can be explained mainly by slight reductions in turbulence below the inversion, rather than changes in κ. As the present simulations at the stratocumulus locations (S11 and S12) have full cloud cover and extend only to $\kappa \sim 0.4$, the effects of evaporative enhancement on stratocumulus cloud feedbacks under conditions, where cloud fraction has a strong dependence on κ, i.e., $\kappa > 0.4-0.5$ [*Moeng*, 2000; *Lock*, 2009], remain to be explored.

A goal of the CGILS LES intercomparisons has to provide benchmark results that could test cloud feedbacks in single column versions of climate models. The present study provides two more benchmarks for which the LES response is robust enough to be a useful constraint. The first CGILS intercomparison showed that SCMs may not respond smoothly to such small perturbations due to locking of inversion height to the vertical grid, switching behavior in parameterizations that can turn on and off. As a result, an SCM may not respond to climate perturbations like its parent GCM, complicating use of these benchmark cases. A better comparison approach might be sample simulations with the GCM of a control and perturbed climate at a particular location or within a particular regime, find the mean difference between the control and perturbed forcings, and perform control and perturbed CGILS-like simulations with one or two LES models with that forcing perturbation. The CGILS LES results suggest that the results from such an approach will be somewhat robust to the LES that is used.

Acronyms

CFMIP	Cloud Feedbacks Model Intercomparison Project.
CGILS	CFMIP/GASS Intercomparison of Large eddy and Single column models.
CMIP3	Third Phase of the Coupled Model Intercomparison Project.
CTEI	Cloud-Top Entrainment Instability.
DALES	Dutch Atmospheric Large-Eddy Simulation.
GASS	Global Atmospheric System Studies.
GCM	global climate model.
LaRC	NASA Langley Research Center Large-Eddy Simulation Model.
LCL	lifting condensation level.
LES	large-eddy simulation.

MOLEMA	Met Office Large Eddy Model w/modified momentum advection.
PBL	Planetary Boundary Layer.
RRTMG	Rapid Radiative Transfer Model for GCM Applications.
SAMA	System for Atmospheric Modeling w/modified scalar advection.
SCM	single column model.
SST	sea surface temperature.
SWCRE	shortwave cloud radiative effect.
UCLA	University of California, Los Angeles Large-Eddy Simulation Model.
WRF	Weather Research and Forecasting Model.

Notation

$\Delta 4CO_2$	difference between 4CO2 and CTRL simulations.
ΔCMIP3	difference between CMIP3 and CTRL simulations.
δLCL_{10}^{90}	$LCL(z=0.9z_i) - LCL(z=0.1z_i)$, where $LCL(z)$ is the lifting condensation levels based on mean boundary-layer properties at the height z.
κ	$=1+c_p\Delta\theta_l/(L\Delta q_t)$ where $\Delta\theta_l$ and Δq_t are across-inversion jumps in liquid water potential temperature and total water, respectively. L and c_p are the latent heat of vaporization and specific heat at constant pressure, respectively.
w_*^3	$=2.5\int_0^{z_i}\overline{w'b'}dz$.
z_i	inversion height, measured as the lowest height where the mean relative humidity is 50%.

Acknowledgments

P.N.B. and C.S.B. acknowledge support from the NSF Science and Technology Center for Multi-Scale Modeling of Atmospheric Processes (CMMAP), led by David Randall and managed by Colorado State University under cooperative agreement ATM-0425247. A.C. was supported by the DOE Atmospheric System Research Program under Interagency agreement DE-SC0005450 and DE-SC0008779 and used computational resources provided by Argonne National Laboratory, DOE's Office of Science and the local computation clusters: K-cluster and Icluster. S.E. was partly supported by the Laboratory Directed Research and Development (LDRD) Program of Brookhaven National Laboratory. T.H. was supported by the Deutscher Wetter Dienst (DWD) through the Hans-Ertel Centre for Weather Research. J.J.v.d.D. was supported by the European Union CLoud Intercomparison, Process Study & Evaluation (EUCLIPSE) project through funding from European Union, Seventh Framework Programme (FP7/2007-2013) under grant agreement 244067. The model output data and scripts used to produce the plots in this paper, along with a description of the simulation setup and forcings for the different cases, may be accessed at http://hdl.handle.net/1773/37295.

References

Blossey, P. N., C. S. Bretherton, M. Zhang, A. Cheng, S. Endo, T. Heus, Y. Liu, A. Lock, S. R. de Roode, and K.-M. Xu (2013), Marine low cloud sensitivity to an idealized climate change: The CGILS LES intercomparison, *J. Adv. Model. Earth Syst.*, *5*, 234–258, doi:10.1002/jame.20025.

Bony, S., and J. Dufresne (2005), Marine boundary layer clouds at the heart of tropical cloud feedback uncertainties in climate models, *Geophys. Res. Lett.*, *32*, L20806, doi:10.1029/2005GL023851.

Bony, S., et al. (2015), Clouds, circulation and climate sensitivity, *Nat. Geosci.*, *8*, 261–268, doi:10.1038/ngeo2398.

Bretherton, C. S. (2015), Insights into low-latitude cloud feedbacks from high-resolution models, *Philos. Trans. R. Soc. A*, *373*, 20140415, doi:10.1098/rsta.2014.0415.

Bretherton, C. S., and P. N. Blossey (2014), Low cloud reduction in a greenhouse-warmed climate: Results from Lagrangian LES of a subtropical marine cloudiness transition, *J. Adv. Model. Earth Syst.*, *6*, 91–114, doi:10.1002/2013MS000250.

Bretherton, C. S., J. Uchida, and P. N. Blossey (2010), Slow manifolds and multiple equilibria in stratocumulus-capped boundary layers, *J. Adv. Model. Earth Syst.*, *2*, 14, doi:10.3894/JAMES.2010.2.14.

Bretherton, C. S., P. N. Blossey, and C. R. Jones (2013), Mechanisms of marine low cloud sensitivity to idealized climate perturbations: A single-LES exploration extending the CGILS cases, *J. Adv. Model. Earth Syst.*, *5*, 316–337, doi:10.1002/jame.20019.

Brient, F., and S. Bony (2012), Interpretation of the positive low-cloud feedback predicted by a climate model under global warming, *Clim. Dyn.*, *40*, 2415, doi:10.1007/s00382-011-1279-7.

Brient, F., and T. Schneider (2016), Constraints on climate sensitivity from space-based measurements of low-cloud reflection, *J. Clim.*, *29*, 5821–5835, doi:10.1175/JCLI-D-15-0897.1.

Caldwell, P., and C. S. Bretherton (2009), Response of a subtropical stratocumulus-capped mixed layer to climate and aerosol changes, *J. Clim.*, *20*, 20–38, doi:10.1175/2008JCLI1967.1.

Cess, R. D., et al. (1990), Intercomparison and interpretation of climate feedback processes in 19 atmospheric general circulation models, *J. Geophys. Res.*, *95*(D10), 16,601–16,615, doi:10.1029/JD095iD10p16601.

Christensen, M. W., G. G. Carrió, G. L. Stephens, and W. R. Cotton (2013), Radiative impacts of free-tropospheric clouds on the properties of marine stratocumulus, *J. Atmos. Sci.*, *70*, 3102–3118, doi:10.1175/JAS-D-12-0287.1.

Clement, A. C., R. Burgman, and J. R. Norris (2009), Observational and model evidence for positive low-level cloud feedback, *Science*, *325*, 460–464, doi:10.1126/science.1171255.

Dal Gesso, S., A. P. Siebesma, S. R. de Roode, and J. M. van Wessem (2014), A mixed-layer model perspective on stratocumulus steady states in a perturbed climate, *Q. J. R. Meteorol. Soc.*, *140*, 2119–2131, doi:10.1002/qj.2282.

De Roode, S. R., A. P. Siebesma, S. Dal Gesso, H. J. J. Jonker, J. Schalkwijk, and J. Sival (2014), A mixed-layer model study of the stratocumulus response to changes in large-scale conditions, *J. Adv. Model. Earth Syst.*, *6*, 1256–1270, doi:10.1002/2014MS000347.

Dessler, A. E. (2010), A determination of the cloud feedback from climate variations over the past decade, *Science*, *330*, 1523–1527, doi:10.1126/science.1192546.

Jones, C. R., C. S. Bretherton, and D. Leon (2011), Coupled vs. decoupled boundary layers in VOCALS-REx, *Atmos. Chem. Phys.*, *11*, 7143–7153, doi:10.5194/acp-11-7143-2011.

Klein, S. A., and D. L. Hartmann (1993), The seasonal cycle of low stratiform clouds, *J. Clim.*, *6*, 1587–1606.

Lock, A. P. (2009), Factors influencing cloud area at the capping inversion for shallow cumulus clouds, *Q. J. R. Meteorol. Soc.*, *135*, 941–952, doi:10.1002/qj.424.

Mlawer, E. J., S. J. Taubman, P. D. Brown, M. J. Iacono, and S. A. Clough (1997), Radiative transfer for inhomogeneous atmospheres: RRTM, a validated correlated-k model for the longwave, *J. Geophys. Res.*, *102*(D14), 16,663–16,682, doi:10.1029/97JD00237.

Moeng, C.-H. (2000), Entrainment rate, cloud fraction, and liquid water path of PBL stratocumulus clouds, *J. Atmos. Sci.*, *57*, 3627–3643.

Myers, T. A., and J. R. Norris (2015), On the relationships between subtropical clouds and meteorology in observations and CMIP3 and CMIP5 models, *J. Clim.*, *28*, 2945–2967, doi:10.1175/JCLI-D-14-00475.1.

Myers, T. A., and J. R. Norris (2016), Reducing the uncertainty in subtropical cloud feedback, *Geophys. Res. Lett.*, *43*, 2144–2148, doi:10.1002/2015GL067416.

Qu, X., A. Hall, S. A. Klein, and P. M. Caldwell (2014), On the spread of changes in marine low cloud cover in climate model simulations of the 21st century, *Clim. Dyn.*, *42*, 2603–2626, doi:10.1007/s00382-013-1945-z.

Qu, X., A. Hall, S. A. Klein, and P. M. Caldwell (2015a), The strength of the tropical inversion and its response to climate change in 18 CMIP5 models, *Clim. Dyn.*, *45*(1), 375–396, doi:10.1007/s00382-014-2441-9.

Qu, X., A. Hall, S. A. Klein, and A. M. DeAngelis (2015b), Positive tropical marine low-cloud cover feedback inferred from cloud-controlling factors, *Geophys. Res. Lett.*, *42*, 7767–7775, doi:10.1002/2015GL065627.

Seifert, A., T. Heus, R. Pincus, and B. Stevens (2015), Large-eddy simulation of the transient and near-equilibrium behavior of precipitating shallow convection, *J. Adv. Model. Earth Syst.*, *7*, 1918–1937, doi:10.1002/2015MS000489.

Tan, Z., T. Schneider, J. Teixeira, and K. G. Pressel (2016), Large-eddy simulation of subtropical cloud-topped boundary layers: 1. A forcing framework with closed surface energy balance, *J. Adv. Model. Earth Syst.*, *8*, doi:10.1002/2016MS000655.

van der Dussen, J. J., S. R. de Roode, S. D. Gesso, and A. P. Siebesma (2015), An LES model study of the influence of the free tropospheric thermodynamic conditions on the stratocumulus response to a climate perturbation, *J. Adv. Model. Earth Syst.*, *7*, 670–691, doi:10.1002/2014MS000380.

Vogel, R., L. Nuijens, and B. Stevens (2016), The role of precipitation and spatial organization in the response of trade-wind clouds to warming, *J. Adv. Model. Earth Syst.*, *8*, 843–862, doi:10.1002/2015MS000568.

Wood, R., and C. S. Bretherton (2006), On the relationship between stratiform low cloud cover and lower-tropospheric stability, *J. Clim.*, *19*, 6425–6432, doi:10.1175/JCLI3988.1.

Zhang, M., C. S. Bretherton, P. N. Blossey, S. Bony, F. Brient, and J.-C. Golaz (2012), The CGILS experimental design to investigate low cloud feedbacks in general circulation models by using single-column and large-eddy simulation models, *J. Adv. Model. Earth Syst.*, *4*, M12001, doi:10.1029/2012MS000182.

Zhang, M., et al. (2013), CGILS: Results from the first phase of an international project to understand the physical mechanisms of low cloud feedbacks in single column models, *J. Adv. Model. Earth Syst.*, *5*, 826–842, doi:10.1002/2013MS000246.